ICIC Express Letters
Volume **17**, Number **11**, November **2023**

ICIC International ©2023 ISSN 1881-803X
pp. **1177–1186**

A COMPARISON OF THREE DEEP LEARNING METHODS FOR PREDICTING LAND SURFACE TEMPERATURE USING LANDSAT 8 IMAGERY

Dion Andres and Sani Muhamad Isa*

BINUS Graduate Program – Master of Computer Science
Bina Nusantara University
Jl. K. H. Syahdan No. 9, Kemanggisan, Palmerah, Jakarta 11480, Indonesia
dion.andres@binus.ac.id; *Corresponding author: sani.m.isa@binus.ac.id

Received November 2022; accepted February 2023

Abstract. *Land Surface Temperature (LST) is a part of temperature that explains the general temperature condition of an environment. A number of variables, including weather, cloud cover, and time spent in the sun, can have an impact on LST. The present LST situation in DKI Jakarta has substantially changed as a result of the pandemic. In the upcoming years, these changes will have an impact on LST prediction. Therefore, the aim of this study is to compare three selected popular deep learning methods to see which one is the most effective at correctly predicting LST changes. Long Short-Term Memory (LSTM), Bidirectional Long Short-Term Memory (BiLSTM), and Convolutional Neural Network with LSTM are chosen to compare each other. The results show that BiLSTM made a higher accurate prediction than other compared models with Root Mean Square Error (RMSE) of 1.08039, Mean Absolute Error (MAE) of 0.79138, Mean Absolute Percentage Error (MAPE) of 0.02959, and Coefficient of Determination (R^2) Score of 0.53124. However, CNN-LSTM is faster in training and predicting based on computing time and provides a decent degree of prediction accuracy with RMSE of 1.21163, MAE of 0.94616, MAPE of 0.03501, and R^2 Score of 0.41045.*

Keywords: Land Surface Temperature, Remote sensing, Urban heat island, LSTM, BiLSTM, CNN-LSTM, Jakarta Province

1. **Introduction.** All aspects of existence are influenced by temperature, which is strongly tied to human life, agricultural productivity, urbanization, and social economics. Studies showed that the increase in global temperature is severe that the change for the average global temperature would increase above 1.5°C over the upcoming four years, from 2023 to 2026, which has increased to almost 50% [1]. It has caused several significant changes especially in agriculture [2], health [3], and economics [4]. However, COVID-19 pandemic has had a significant impact on the world, requiring restrictions on human activity in order to slow the virus' spread. These restrictions trigger an unexpected temperature change in Indonesia, notably in Indonesia capital city.

The Land Surface Temperature (LST) condition in DKI Jakarta has undergone a significant change during the pandemic. Before the pandemic, the average of LST in DKI Jakarta could reach more than 33°C with the highest temperature exceeding 36°C [5]. The increase in temperature occurred due to the urbanization and community activities. Some researchers predicted that the trend of rising temperatures in Jakarta would continue in the coming years, reflecting the rise in global temperatures [6]. However, the pandemic occurred in 2020 throughout the world including Indonesia which caused a decrease in human activities, especially in the industrial sectors and transportation activities. As a result, the LST decreased to around 23°C-29°C [7]. These changes will influence LST prediction in the coming years. Accurate LST prediction could provide useful information to

DOI: 10.24507/icicel.17.11.1177

urban planners, agriculturists, medical professionals, and other business planners; however, LST prediction is difficult due to a variety of uncertain relevant factors. Furthermore, only few researchers use deep learning to predict LST.

Several popular deep learning models such as Long Short-Term Memory (LSTM), Convolutional Neural Network (CNN), and Bidirectional Long Short-Term Memory (Bi-LSTM) are often used in several fields due to their high performance depending on conditions. Despite that, the use of deep learning models in the LST field, especially with Landsat Imagery Satellite data is still limited. First, Kartal and Sekertekin proposed a model named Convolutional LSTM to predict LST using MODIS Satellite Imagery and the result is that the proposed model could be used for one step ahead spatiotemporal prediction of LST data [8]. Second, Maddu et al. proposed a hybrid model named LSTM-BiLSTM to predict the major coastal cities of India and the result is that proposed hybrid model was effective in predicting LST of coastal cities of India [9]. Besides that, Khalil et al. used LSTM model to predict the LST where the result is that LSTM model achieved higher efficiency than Artificial Neural Network [10]. While several deep learning methods have been used to predict the LST, there is still no best model that can accurately predict the LST under the same condition (same study area, similar weather, size of data, etc.). Due to the fact that the training also affected from characteristics of certain areas, some models with specific parameter tuning may be the best in one study area but not in another. Additionally, there are only a few studies that used pixels as input data for prediction such as Jia et al.'s experiment [11], although each pixel represents LST value for fixed area and can be easily visualized (both input and output visualization). Hence, the goal of this study is to find the best deep learning methods from three chosen methods for accurately predicting LST pixels change. LSTM, BiLSTM, and CNN-LSTM are chosen due to their popularity from all deep learning models. It is hoped that through this research, it is possible to provide information regarding each method's performance in predicting the LST with the same dataset. This information can be considered for further research.

This paper is organized as follows: Section 2 describes the study area and materials, Section 3 describes the methods, Section 4 describes the results and discussion, Section 5 describes the conclusion and the future works.

2. **Study Area and Materials.**

2.1. **Study area.** DKI Jakarta Province is located in the northwest part of Java Island and near the equator (Figure 1). Its position is approximately between 5°19′12″-6°23′54″ South Latitude and 106°22′42″-106°58′18″ East Longitude. It has a total land area of 661.52 km^2 and there are around 110 islands scattered in Thousand Islands (*Kepulauan Seribu*). Administratively, DKI Jakarta Province is divided into five municipalities and one administrative district, namely Central Jakarta, North Jakarta, East Jakarta, South Jakarta, West Jakarta, and Thousand Islands Administrative District.

2.2. **Data.** Landsat 8 Satellite Imagery generates an image of the Earth in a repeating cycle of 16 days by collecting multiple satellite images. A total of 11 bands are collected by two specific sensors on the Landsat 8 satellite, which are Operational Land Imager (OLI) and Thermal Infrared Sensor (TIRS). There are two bands from OLI sensor that were used in this study, which are band 4 (Red) and band 5 (Near-infrared). Furthermore, there is one band from TIRS sensor that becomes a main data for this study, which is band 10 (TIRS 1).

The Land Surface Temperature (LST) data for training and testing are obtained from Landsat 8 Satellite Imagery and the locations are North Jakarta, East Jakarta, South Jakarta, West Jakarta, and Central Jakarta. Specifically, the data are taken from Landsat 8 OLI/TIRS Collection 2 Level-1 satellite imagery result with the path-row from 122 to 64.

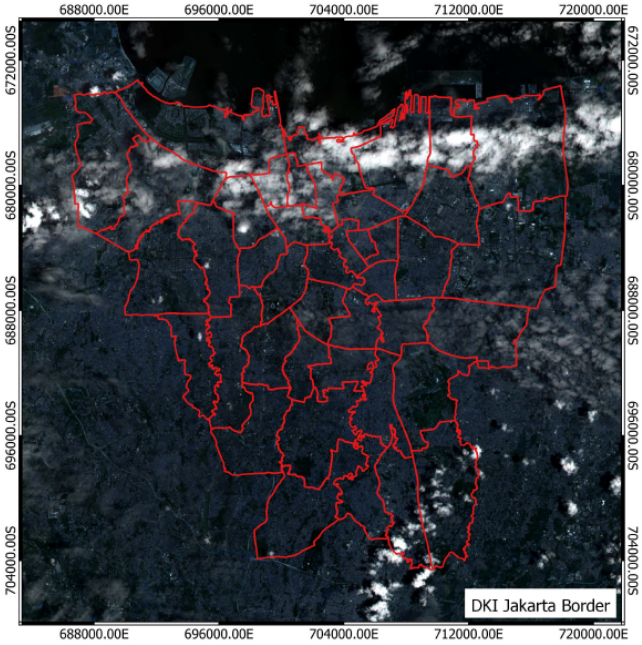

FIGURE 1. DKI Jakarta Province (Without Thousand Islands)

The selected data are taken from every month from January 2016 to August 2022 and will be overall cloud free since the LST will be affected by several factors like cloud temperature or radiation reflection induced by clouds. The data used were downloaded from the United States Geological Survey (USGS) web page (https://earthexplorer.usgs.gov).

3. **Methods.** The research process has three main steps after the materials have been collected. First, Land Surface Temperature (LST) is calculated using the materials. Second, each related deep learning model is constructed to process the LST data including parameter tuning. Lastly, each model is evaluated with corresponding evaluation metrics.

3.1. **Land Surface Temperature (LST) calculation.** LST is a crucial factor in overcoming surface energy budget assessments, and it is usually measured using remote sensing [12]. LST is influenced by four main factors, namely Top of Atmosphere (TOA) Spectral Radiance, Brightness Temperature (BT), Normalized Difference Vegetation Index (NDVI), and Land Surface Emissivity (LSE) [13].

The first step to calculate the LST starts from measuring the TOA Spectral Radiance, which is the light reflected from the ground and measured from the atmosphere [14]. The formula is based on the USGS tools [15] and is as follows:

$$L\lambda = M_L * Q_{cal} + A_L - O_i, \tag{1}$$

where M_L is the band-specific multiplicative rescaling factor, Q_{cal} is band 10 image, A_L is the band-additive rescaling factor, and O_i is the correction for band 10.

The result of the TOA Spectral Radiance calculation is used to calculate BT, which is the second step. The thermal constants provided in the metadata file should be used to convert the TIRS band data from spectral radiance to Brightness Temperature (BT) [16]. The formula is as follows:

$$BT = \frac{K2}{\ln\left[\left(\frac{K1}{L\lambda}\right) + 1\right]} - 273.15, \tag{2}$$

where $K1$ and $K2$ are the thermal conversion constants for the corresponding band that are listed in the metadata file of the satellite image, $L\lambda$ are the TOA Spectral Radiance, and the radiant temperature must be adjusted by applying absolute zero, or about $-273.15°$C, in order to output the result in Celsius.

The third step is to calculate NDVI, since the amount of vegetation present is a crucial factor and the NDVI can be used to infer general vegetation condition [17]. NDVI is a crucial value due to its strong correlation with the Proportion of Vegetation (P_v) and Emissivity (ε), which are used to calculate LST:

$$NDVI = \frac{NIR(band\ 5) - R(band\ 4)}{NIR(band\ 5) + R(band\ 4)}, \tag{3}$$

where NIR is the near-infrared band (Band 5) and R is the red band (Band 4).

P_v is the ratio of the vertical projection area of vegetation on the ground [18]. There are two NDVI values used to calculate P_v, which are vegetation pixel thresholds (maximum NDVI value, $NDVI_v$) and soil pixel threshold (minimum NDVI value, $NDVI_s$) [19], so the formula is as follows [20]:

$$P_v = \left(\frac{NDVI - NDVI_s}{NDVI_v - NDVI_s}\right)^2, \tag{4}$$

where $NDVI_v$ and $NDVI_s$ can be obtained from (3), since the output is a series of numbers.

The LSE must be calculated in order to estimate LST, since the LSE is a proportionality factor that scales blackbody radiance (Planck's law) to forecast emitted radiance, and it is the efficiency of transporting heat energy over the surface into the atmosphere [21]. The formula to compute LSE is as follows [20]:

$$\varepsilon_\lambda = \varepsilon_{v\lambda} P_v + \varepsilon_{s\lambda}(1 - P_v) + C_\lambda, \tag{5}$$

where $\varepsilon_{v\lambda}$ is the vegetation, $\varepsilon_{s\lambda}$ is soil emissivity, P_v represents the Proportion of Vegetation, and C_λ represents the surface roughness.

The last step of calculating the LST is computed as follows [13,21]:

$$T_s = \frac{BT}{\{1 + [(\lambda BT/\rho)\ln \varepsilon_\lambda]\}}, \tag{6}$$

where T_s is the LST in Celcius (°C), BT is Brightness Temperature which is calculated in (2), λ is the wavelength of emitted radiance, ε_λ represents the emissivity calculated in (5), and

$$\rho = h\frac{c}{\sigma} = 1.438 \times 10^{-2}\ \text{mK}, \tag{7}$$

where σ represents the Boltzmann constant (1.38×10^{-23} J/K), h is Planck's constant (6.626×10^{-34} J/s), and c is the light velocity (2.998×10^8 m/s).

3.2. **Deep learning models.** Three deep learning models that were used in this study are Long Short-Term Memory (LSTM), Bidirectional Long Short-Term Memory (Bi-LSTM), and Convolutional Neural Network with Long Short Term Memory (CNN-LSTM). Each of these model nodes is tuned four times: 32 nodes, 64 nodes, 128 nodes, and 256 nodes, respectively. Each model is trained for 100 epochs, which is a common approach for deep learning model training. Additionally, the input dataset used is LST data in the form of pixel, since the objective of study is to predict the LST pixel itself according to the study area. Each of pixel is regarded as a feature in the model.

3.2.1. *LSTM.* LSTM is a Recurrent Neural Network (RNN) extension that is capable of learning long-term dependencies, especially in sequence prediction problems. LSTM was developed to address issues with long-term learning in RNN caused by the Vanishing Gradient Problem [23]. Unlike RNN, LSTM adds a forget gate, an input gate, and an update gate to forget and update information to the cell state [24]. Figure 2 shows the LSTM model architecture that is used in this study.

There are two layers with the same neuron units. These LSTM layers attempt to factor LST value changes by using the information from LST Pixel Data stored in its memory cell, which consists of the three gates (input, forget, and output). Additionally, there is

FIGURE 2. LSTM model architecture

a dense layer that receives data from the preceding layer in its entirety. This dense layer learns features from all combinational features of the previous layer.

3.2.2. *BiLSTM.* BiLSTM, also known as Bidirectional RNN, is a combination between two LSTM models that combine information from the input sequence in both forward and backward directions, allowing it to better grasp bidirectional semantic relationships [25]. At first, LSTM units can make predictions based on past data but not on future data. BiLSTM overcomes this limitation. BiLSTM structure allows for the use of both backward and forward information. Figure 3 shows the BiLSTM model architecture that is used in this study.

FIGURE 3. BiLSTM model architecture

There are two layers with identical neuron units, one dense layer and one output layer, similar to LSTM. However, the BiLSTM structure differs in that it has two states: Forward State and Backward State. By combining the outputs of both directions, memory can record information from both ends of the state in relation, improving prediction accuracy. Therefore, BiLSTM can learn the dataset from both states while LSTM only can learn it from one state.

3.2.3. *CNN-LSTM.* A hybrid CNN-LSTM consists of CNN and LSTM itself. CNN is a deep learning model that is mostly used to extract spatial information from large datasets [26], while LSTM was designed to learn temporal properties from time series or sequential data. The basic idea to combine CNN and LSTM is that CNN model extracts the spatial contextual elements of surrounding temperatures, while the LSTM model extracts the temporal features. Both models will be concatenated, and parameter tuning will be performed.

Among the many CNN designs available, AlexNet was selected for this study because it has a faster training speed than other CNN architectures and a deeper architecture with 8 layers, which implies it can extract features more successfully. In this study, AlexNet is used to extract spatial features, particularly from surrounding pixels, from the LST dataset. LSTM would then accept the input from AlexNet and use its sequence data to learn the temporal characteristic. The output is the same as LSTM and BiLSTM. Figure 4 shows the CNN-LSTM model architecture that is used in this study.

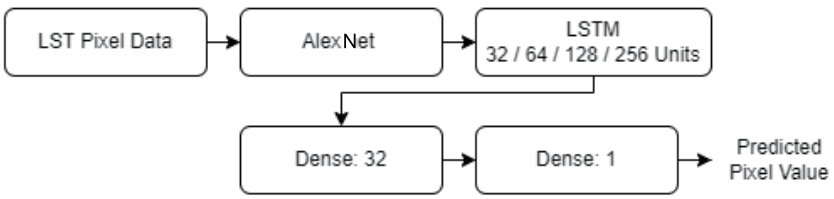

FIGURE 4. CNN-LSTM model architecture

3.3. **Evaluation metrics.** The most crucial part of model experiment is metric evaluation, which is used to compare models that have been employed [27]. Root Mean Square Error (RMSE), Mean Absolute Error (MAE), Mean Absolute Percentage Error (MAPE), and Coefficient of Determination (R^2) are used in this study. Each evaluation index's equation is as follows.

$$RMSE = \sqrt{\frac{\sum_{t=1}^{n} \|e_t - e'_t\|^2}{n}}, \tag{8}$$

$$MAE = \frac{\sum_{t=1}^{n} |e'_t - e_t|}{n}, \tag{9}$$

$$MAPE = \frac{1}{n} \sum_{t=1}^{n} \left| \frac{e_t - e'_t}{e_t} \right|, \tag{10}$$

$$R^2 = 1 - \frac{\sum_{i=0}^{n} (e'_i - e_i)^2}{\sum_{i=0}^{n} (e_i \bar{e})^2}, \tag{11}$$

where e is the ground truth, e' is the predicted value, $\bar{e}$ is the mean value, and n is the number of data used in the testing.

4. Results and Discussion.

4.1. **Results.** Evaluation metrics are applied to the predicted and actual LST values, providing the RMSE, MAE, MAPE, and R^2 Score for each model, which are presented in Table 1 for comparison. Furthermore, computational time is also included as well to compare each model in terms of time performance.

Table 1. Model evaluation metric score

Model	Nodes	Metric score				Computational time
		RMSE	MAE	MAPE	R^2 Score	
BiLSTM	32	1.08039	0.79138	0.02959	0.53124	23.10 hours
	64	1.12131	0.84149	0.03137	0.49507	31.30 hours
	128	1.12611	0.84399	0.03149	0.49073	43.07 hours
	256	1.14834	0.86516	0.03224	0.47043	59.70 hours
LSTM	32	1.11610	0.83101	0.03102	0.49974	17.41 hours
	64	1.09266	0.80562	0.03011	0.52054	21.40 hours
	128	1.11421	0.83213	0.03110	0.50144	42.21 hours
	256	1.15574	0.87471	0.03256	0.46359	53.67 hours
CNN-LSTM	32	1.21163	0.94616	0.03501	0.41045	15.09 hours
	64	1.42950	1.20792	0.04439	0.17937	15.35 hours
	128	1.22026	0.95293	0.03528	0.40202	15.11 hours
	256	1.36150	1.12869	0.04155	0.25580	15.47 hours

In terms of overall prediction error, the BiLSTM with 32 nodes surpasses other BiLSTM, with RMSE of 1.08039, MAE of 0.79138, MAPE of 0.02959, and R^2 Score of 0.53124. Meanwhile, LSTM with 64 nodes outperforms other LSTM, with outcomes as RMSE of 1.09266, MAE of 0.80562, MAPE of 0.03011, and R^2 Score of 0.50144. Finally, a CNN-LSTM with 32 nodes has a smaller prediction error than other CNN-LSTM models, with values as RMSE of 1.21163, MAE of 0.94616, MAPE of 0.03501, and R^2 Score of 0.41045.

The BiLSTM model is the best model when comparing the prediction errors of the three top models since each of its model evaluation scores is higher than those of the other models. On the other hand, CNN-LSTM is faster during training and offers a respectable

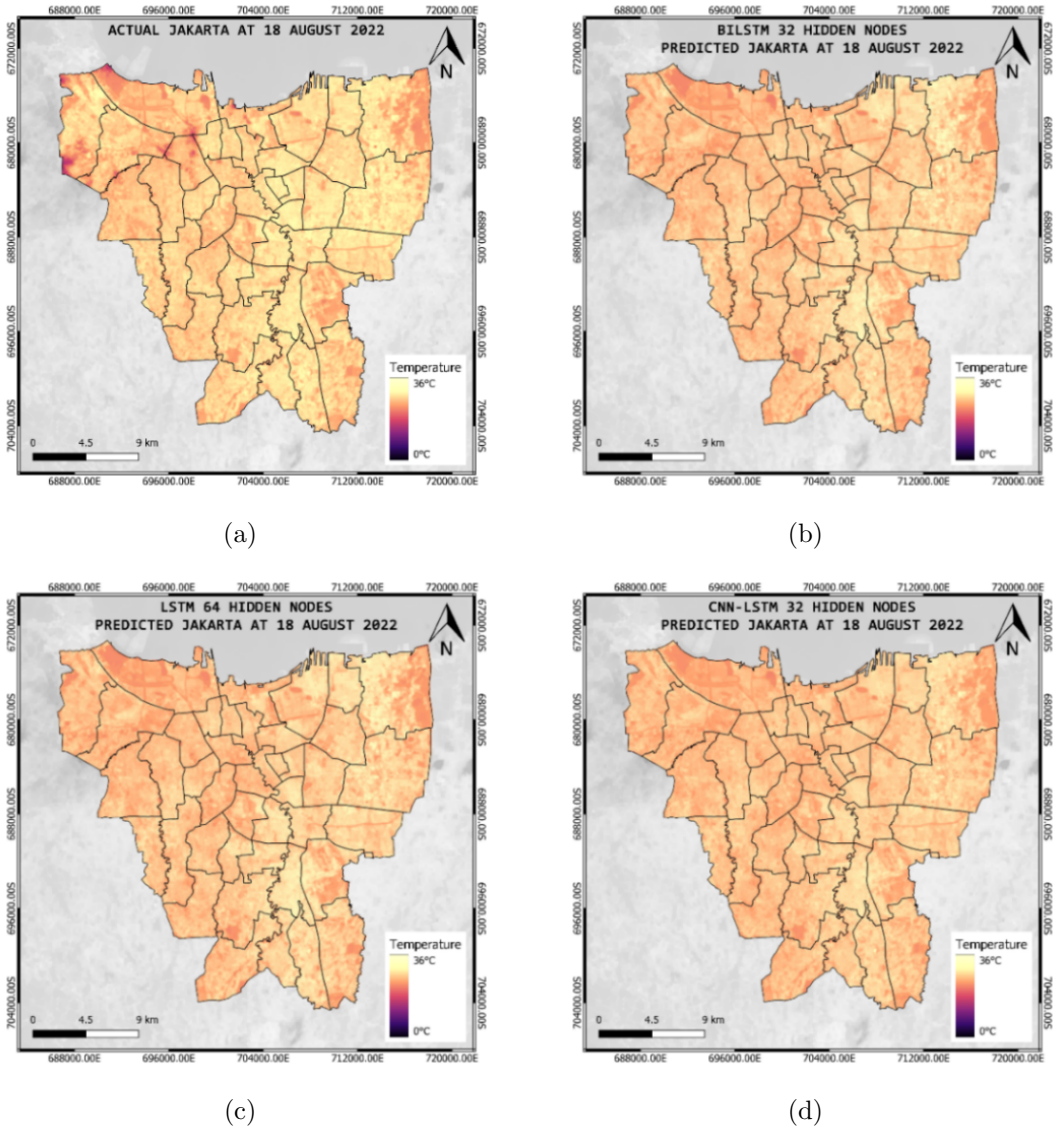

FIGURE 5. (color online) LST visualization: (a) Actual, (b) BiLSTM prediction, (c) LSTM prediction, and (d) CNN-LSTM prediction

level of prediction accuracy. Figure 5 shows the prediction results from each of the best models when compared to real LST time series data.

4.2. **Discussion.** According to the data, the three best models do a great job of predicting LST at DKI Jakarta, with CNN-LSTM coming in as the fastest computational model and BiLSTM coming in as the model with the lowest error percentage. CNN-LSTM has a faster computational time than others since it can learn two aspects simultaneously, spatial and temporal. While LSTM learns the temporal from sequential data based on retrieved spatial information, CNN can extract most of the spatial information that is similar to image information. In other words, CNN-LSTM can learn and predict spatio-temporal data. In contrast, BiLSTM's prediction accuracy is better than others since it incorporates data from both forward and backward directions. BiLSTM concentrated on learning the temporal characteristic from each pixel in the LST data, even if it was unable to adequately extract spatial information. For greater accuracy in forecasting the LST in pixels, BiLSTM combines the sequential data in forward and backward order that it has learned. However, the more data used, the longer BiLSTM takes to learn and predict it, since BiLSTM only focused on each pixel.

Furthermore, both models are capable of accurately predicting areas with high temperatures as shown on Figure 5. However, neither model can provide an accurate prediction in areas with low temperatures, particularly those that are cloud-covered. In order to provide more information, MAE for each pixel is generated and plotted in the same manner as the predicted results in the form of the DKI Jakarta map. Figure 6 shows the error spread of the BiLSTM and CNN-LSTM models based on the minimum and maximum range of absolute error, which were derived from each pixel based on the MAE to the actual LST data at relevant date.

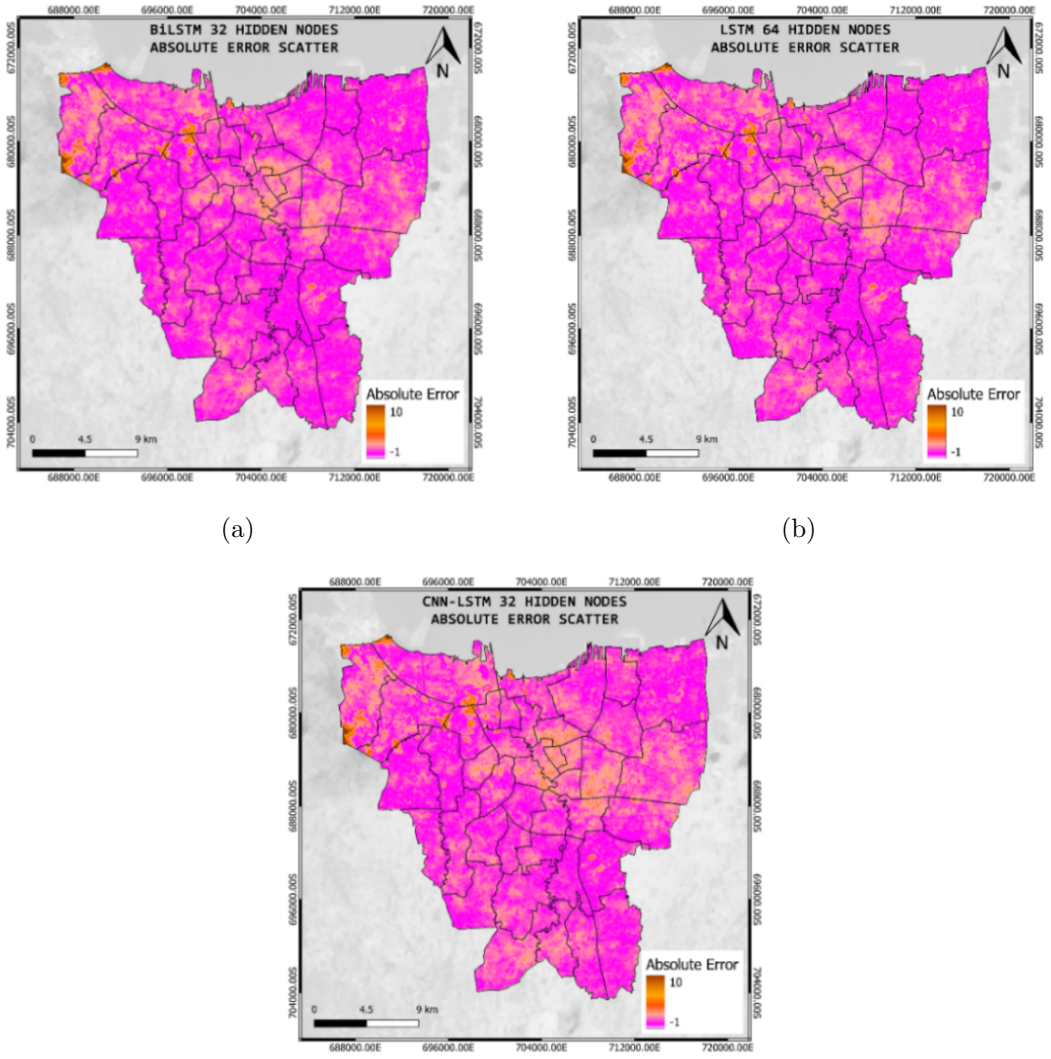

(a) (b)

(c)

FIGURE 6. (color online) Absolute error visualization: (a) BiLSTM, (b) LSTM, and (c) CNN-LSTM

When comparing Figures 5 and 6, each absolute error scatter shows clearly that places with low temperatures have a bigger error result in multiple larger brown areas. Some cloud covers cause some small dark brown spots that represent the highest error score. Meanwhile, the area with high temperatures has a smaller error in the majority of purple locations. There is a resemblance pattern between the error patterns in Figures 6(a), 6(b), and 6(c). This resemblance pattern shows that areas with lower temperatures and significant cloud cover yield higher prediction error rates.

For a more thorough study, Table 2 is created by converting Figure 5 into a table, which displays the total number of pixels that are divided into six distinct temperature ranges.

Table 2. LST pixel count comparison for DKI Jakarta on 18th August 2022

Temperature range (°C)	Pixel count			
	Actual	**BiLSTM**	**LSTM**	**CNN-LSTM**
0.0°C-5.9°C	0	0	0	0
6.0°C-11.9°C	0	0	0	0
12.0°C-17.9°C	977	0	0	0
18.0°C-23.9°C	23057	16336	20676	12597
24.0°C-29.9°C	685421	695028	691947	700557
30.0°C-35.9°C	3924	2015	756	225

Table 2 shows that when predicted by BiLSTM, LSTM, and CNN-LSTM, 0.14% of real pixels with temperature between 12.0°C and 17.9°C become zero. This result was obtained because the majority of pixel counts correspond to temperatures between 24.0°C and 29.9°C, which can be considered as imbalanced data [28]. In addition, three models provided results that were comparable: BiLSTM predicted 97.43%, LSTM predicted 96.99%, and CNN-LSTM predicted 98.20%, which spreads between temperatures in the range of 24.0°C and 29.9°C. Although the results are comparable, the temperature between 30.0°C and 35.9°C is noticeably different. BiLSTM shows results that are more similar to the actual compared to other models.

5. **Conclusion.** The Land Surface Temperature (LST) is one of the most important essential climate variables that have several impacts towards all aspects of life. Hence, an accurate LST prediction becomes an important factor. This paper's objective is to find the best deep learning methods from three chosen popular methods for accurately predicting LST changes based on LST data obtained from Landsat 8 OLI/TIRS satellite imagery. The results show that 32 nodes BiLSTM made a higher accurate prediction than other compared models, with RMSE of 1.08039, MAE of 0.79138, MAPE of 0.02959, and R^2 Score of 0.53124. However, 32 nodes CNN-LSTM is faster during training in terms of computing time and provides a decent degree of prediction accuracy with RMSE of 1.21163, MAE of 0.94616, MAPE of 0.03501, and R^2 Score of 0.41045. Furthermore, areas with lower temperatures, particularly those that are cloud-covered, have larger error values than those with higher temperatures in terms of prediction error. Therefore, while considering time and resources, CNN-LSTM model is a good option for LST prediction. Otherwise, BiLSTM is a sensible option for reliably predicting LST.

Both models require more time and resources to analyze the input data to achieve that result, particularly when the pixel number is large. The larger the study region, the longer it takes the model to train and forecast new pixel values. It is possible to develop a new model that is more compact, provides comparable results, and has the potential to be more efficient in terms of processing load and total time consumption.

REFERENCES

[1] World Meteorological Organization, *50:50 Chance of Global Temperature Temporarily Reaching 1.5°C Threshold in Next Five Years*, https://public.wmo.int/en/media/press-release/wmo-update-5050-chance-of-global-temperature-temporarily-reaching-15°c-threshold, 2022.

[2] G. S. Malhi, M. Kaur and P. Kaushik, Impact of climate change on agriculture and its mitigation strategies: A review, *Sustainability*, vol.13, no.3, 1318, 2021.

[3] G. Benelli, A. B. B. Wilke, J. R. Bloomquist, N. Desneux and J. C. Beier, Overexposing mosquitoes to insecticides under global warming: A public health concern?, *Sci. Total Environ.*, vol.762, 143069, 2021.

[4] K. Desmet and E. Rossi-Hansberg, On the spatial economic impact of global warming, *J. Urban Econ.*, vol.88, pp.16-37, 2015.

[5] A. Saputra, M. H. Ibrahim, S. Shofirun, A. Saifuddin and K. Furoida, Assessing urban heat island in Jakarta, Indonesia during the pandemic of COVID-19, *IOP Conference Series: Earth and Environmental Science*, vol.986, no.1, 012069, 2022.
[6] C. D. Putra, A. Ramadhani and E. Fatimah, Increasing Urban Heat Island area in Jakarta and it's relation to land use changes, *IOP Conference Series: Earth and Environmental Science*, vol.737, no.1, 12002, 2021.
[7] J. Pangesta, D. Andres and M. S. Isa, A comparison of estimated land surface temperature form Landsat 8 between DKI Jakarta and Pekat Village, *ICIC Express Letters*, vol.17, no.4, pp.489-496, 2023.
[8] S. Kartal and A. Sekertekin, Prediction of MODIS land surface temperature using new hybrid models based on spatial interpolation techniques and deep learning models, *Environ. Sci. Pollut. Res.*, pp.1-20, 2022.
[9] R. Maddu, A. R. Vanga, J. K. Sajja, G. Basha and R. Shaik, Prediction of land surface temperature of major coastal cities of India using bidirectional LSTM neural networks, *J. Water Clim. Chang.*, vol.12, no.8, pp.3801-3819, doi: 10.2166/wcc.2021.460, 2021.
[10] U. Khalil et al., Developing a spatiotemporal model to forecast land surface temperature: A way forward for better town planning, *Sustainability*, vol.14, no.19, 11873, 2022.
[11] H. Jia, D. Yang, W. Deng, Q. Wei and W. Jiang, Predicting land surface temperature with geographically weighed regression and deep learning, *Wiley Interdiscip. Rev. Data Min. Knowl. Discov.*, vol.11, no.1, e1396, 2021.
[12] I. F. Trigo, I. T. Monteiro, F. Olesen and E. Kabsch, An assessment of remotely sensed land surface temperature, *J. Geophys. Res. Atmos.*, vol.113, no.17, pp.1-12, doi: 10.1029/2008JD010035, 2008.
[13] U. Avdan and G. Jovanovska, Algorithm for automated mapping of land surface temperature using LANDSAT 8 satellite data, *J. Sensors*, vol.2016, doi: 10.1155/2016/1480307, 2016.
[14] V. C. E. Laurent, W. Verhoef, J. G. P. W. Clevers and M. E. Schaepman, Estimating forest variables from top-of-atmosphere radiance satellite measurements using coupled radiative transfer models, *Remote Sens. Environ.*, vol.115, no.4, pp.1043-1052, 2011.
[15] J. A. Barsi, J. R. Schott, S. J. Hook, N. G. Raqueno, B. L. Markham and R. G. Radocinski, Landsat-8 thermal infrared sensor (TIRS) vicarious radiometric calibration, *Remote Sens.*, vol.6, no.11, pp.11607-11626, 2014.
[16] H. Xu and B. Chen, Remote sensing of the urban heat island and its changes in Xiamen City of SE China, *J. Environ. Sci.*, vol.16, no.2, pp.276-281, 2004.
[17] Q. Weng, D. Lu and J. Schubring, Estimation of land surface temperature-vegetation abundance relationship for urban heat island studies, *Remote Sens. Environ.*, vol.89, no.4, pp.467-483, doi: 10.1016/j.rse.2003.11.005, 2004.
[18] J. W. Deardorff, Efficient prediction of ground surface temperature and moisture, with inclusion of a layer of vegetation, *J. Geophys. Res.*, vol.83, no.C4, 1889, doi: 10.1029/jc083ic04p01889, 1978.
[19] F. Wang, Z. Qin, C. Song, L. Tu, A. Karnieli and S. Zhao, An improved mono-window algorithm for land surface temperature retrieval from Landsat 8 thermal infrared sensor data, *Remote Sens.*, vol.7, no.4, pp.4268-4289, 2015.
[20] J. A. Sobrino, J. C. Jiménez-Muñoz and L. Paolini, Land surface temperature retrieval from LANDSAT TM 5, *Remote Sens. Environ.*, vol.90, no.4, pp.434-440, 2004.
[21] J. C. Jiménez-Muñoz, J. A. Sobrino, A. Gillespie, D. Sabol and W. T. Gustafson, Improved land surface emissivities over agricultural areas using ASTER NDVI, *Remote Sens. Environ.*, vol.103, no.4, pp.474-487, 2006.
[22] M. Stathopoulou and C. Cartalis, Daytime urban heat islands from Landsat ETM+ and Corine land cover data: An application to major cities in Greece, *Sol. Energy*, vol.81, no.3, pp.358-368, 2007.
[23] Y. Yu, X. Si, C. Hu and J. Zhang, A review of recurrent neural networks: LSTM cells and network architectures, *Neural Comput.*, vol.31, no.7, pp.1235-1270, 2019.
[24] S. Hochreiter and J. Schmidhuber, Long short-term memory, *Neural Comput.*, vol.9, no.8, pp.1735-1780, 1997.
[25] M. Schuster and K. K. Paliwal, Bidirectional recurrent neural networks, *IEEE Trans. Signal Process.*, vol.45, no.11, pp.2673-2681, 1997.
[26] M. Reichstein, G. Camps-Valls, B. Stevens, M. Jung, J. Denzler and N. Carvalhais, Deep learning and process understanding for data-driven Earth system science, *Nature*, vol.566, no.7743, pp.195-204, 2019.
[27] N. Japkowicz and M. Shah, Performance evaluation in machine learning, *Mach. Learn. Radiat. Oncol. Theory Appl.*, pp.41-56, 2015.
[28] J. M. Johnson and T. M. Khoshgoftaar, Survey on deep learning with class imbalance, *J. Big Data*, vol.6, no.1, pp.1-54, 2019.